# Homogeneous Crystallization in Cyclically Sheared Frictionless Grains

Weiwei Jin,[1,*] Corey S. O'Hern,[1,2,3] Charles Radin,[4] Mark D. Shattuck,[5] and Harry L. Swinney[6]
[1]Department of Mechanical Engineering and Materials Science, Yale University, New Haven, Connecticut 06520, USA
[2]Department of Physics, Yale University, New Haven, Connecticut 06520, USA
[3]Department of Applied Physics, Yale University, New Haven, Connecticut 06520, USA
[4]Department of Mathematics, University of Texas at Austin, Austin, Texas 78712, USA
[5]Benjamin Levich Institute and Physics Department, The City College of New York, New York, New York 10031, USA
[6]Center for Nonlinear Dynamics and Department of Physics, University of Texas at Austin, Austin, Texas 78712, USA

(Received 4 August 2020; accepted 20 November 2020; published 18 December 2020)

Many experiments over the past half century have shown that, for a range of protocols, granular materials compact under pressure and repeated small disturbances. A recent experiment on cyclically sheared spherical grains showed significant compaction via homogeneous crystallization (Rietz *et al.*, 2018). Here we present numerical simulations of frictionless, purely repulsive spheres undergoing cyclic simple shear via Newtonian dynamics with linear viscous drag at fixed vertical load. We show that for sufficiently small strain amplitudes, cyclic shear gives rise to homogeneous crystallization at a volume fraction $\phi = 0.646 \pm 0.001$. This result indicates that neither friction nor gravity is essential for homogeneous crystallization in driven granular media. Understanding how crystal formation is initiated within a homogeneous disordered state gives key insights into the old open problem of glass formation in fluids.

DOI: 10.1103/PhysRevLett.125.258003

Loose granular materials will compact for a range of different protocols of small repeated disturbances while under the influence of gravity and/or external pressure. In the half century following the pioneering work of Bernal [1] and Scott [2], the existence of a barrier to compaction has been confirmed for many types of disturbances [3–6], but not for cyclic shear for which the systems compacted via wall-induced crystallization [7,8]. Walls that inhibit nucleation and precision measurements of the positions of the spherical grains recently enabled Rietz *et al.* [9] to observe homogeneous crystallization in a granular material undergoing cyclic shear.

Using Newtonian dynamics with linear viscous drag, we numerically simulate purely repulsive spherical grains undergoing cyclic simple shear strain to model granular crystallization as found in the Rietz *et al.* experiment [9]. The simulations allow us to tune the grain interactions, gravity, and boundary conditions to understand the essential physics that gives rise to homogeneous crystallization. In a broader context, understanding how crystal formation is initiated within a homogeneous disordered state is one of the fundamental questions in the old open problem of glass formation in fluids [10–16].

Our simulations reveal the essential physical requirements needed for crystallization in driven, dissipative granular materials: volume exclusion, system confinement, and small disturbances that allow grain rearrangements. In particular, gravity, friction, and energy conservation are not required to yield homogeneous crystallization. Our simulations use deterministic dynamics in contrast with the probabilistic evolution equations used in classical nucleation theory to model crystallization in atomic and molecular systems [17,18].

The simulations show that the volume fraction at the onset of crystallization becomes independent of the shear amplitude for sufficiently small amplitudes, $A \leq 0.05$ rad, consistent with Rietz *et al.* [9], who used $A = 0.01$ rad. The volume fraction at the onset of crystallization is also within the range of jamming volume fractions found for different packing generation protocols for frictionless hard spheres [19].

*Methods*.—We simulate cyclic simple shear of frictionless monodisperse spheres in three spatial dimensions using the discrete element method (see Supplemental Material, Sec. B [20]). Figure 1(a) shows the simulation cell, designed to mimic the shear cell used in experiments [7,8] with two sidewalls that tilt with respect to the vertical axis by a variable angle $\theta$ in the $x$-$y$ plane, and a bottom wall that oscillates horizontally and can move vertically under an applied load. The initial jammed packing is prepared via gravitational deposition by pouring the grains into a static container and allowing dissipative forces to remove the kinetic energy in the system. A subsystem of size $(L + 2d) \times (1.675)L \times L$ is cut out from the initial packing [see Fig. 1(b)]. Grains with center positions less than $d$ away from all of the surfaces of the subsystem except the two in the $z$ direction (which has periodic boundary conditions) are then fixed to form the walls. Wall-induced crystallization is suppressed since the grains forming the walls are randomly positioned. With $L = 20d$,

 

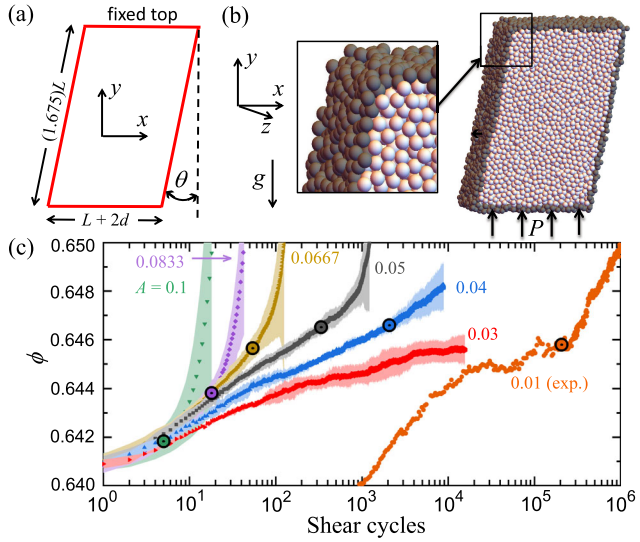


FIG. 1. (a) Cell of dimensions $(L+2d)\times(1.675)L\times L$ used in the simulations of frictionless spheres of diameter $d$ undergoing cyclic shear with $\theta = A\sin(\omega t)$. (b) To inhibit crystallization, the dark colored spheres on the cell boundaries are fixed in disordered positions; the boundary conditions in the $z$ direction are periodic. The light-colored spheres in the interior of the shear cell move in response to interactions with one another, the dark spheres, and gravity $g$. A constant pressure $P$ is applied on the cell bottom, which can move up and down. (c) The volume fraction $\phi$ as a function of cycle number, from simulations with shear amplitudes $A$. The orange points are from an experiment with $A = 0.01$ [9]; at the start of that experiment $\phi = 0.627$, and after 970 shear cycles, $\phi$ had increased to 0.640, which is the first experimental point shown here. The black circles with a colored interior show for each $A$ the value of $\phi$ at the onset of rapid growth of crystallites, as discussed in the results.

the cell contains 18 200 spheres in the interior. In Supplemental Material, Sec. C [20] we show that results obtained for as few as 6000 spheres yield (within the statistical uncertainty) behavior in agreement with the results obtained with 18 200 spheres. The simulation parameters were number of time steps per cycle, 45 600 (for other numbers of time steps, see Supplemental Material, Sec. B.4 [20]); time step, 2 s; grain mass, $2\times10^{-5}$ kg; grain diameter, 3 mm; spring constant, $k = 654$ N/m; damping constant, $b = 1.28\times10^{-3}$ kg/s; and pressure $P = 954$ Pa.

The grains are modeled as frictionless spheres interacting via the pairwise, purely repulsive linear spring force,

$$\vec{F}_{ij} = kd\delta_{ij}\Theta(\delta_{ij})\hat{r}_{ij}, \tag{1}$$

where $k$ is the spring constant (see Supplemental Material, Sec. B.2 [20]), $\delta_{ij} = 1 - r_{ij}/d$ is the intergrain overlap, $r_{ij}$ is the center-to-center separation between grains $i$ and $j$, $\Theta(x)$ is the Heaviside step function, and $\hat{r}_{ij}$ is the unit vector pointing from the center of grain $j$ to the center of grain $i$. The interaction between the fixed wall grains and the interior grains follows the same force law as that between pairs of interior grains. Newton's equation of motion for each interior grain $i$ is

$$m_i\vec{a}_i = \sum_{j=1}^{n_i}\vec{F}_{ij} - b(\vec{v}_i - \vec{v}_{\rm fluid}) - m_i g\hat{y}, \tag{2}$$

where $g\hat{y}$ is the acceleration due to gravity, $m_i$, $\vec{a}_i$, and $\vec{v}_i$ are the mass, acceleration, and velocity of grain $i$, $n_i$ is the number of grains overlapping grain $i$, and $b$ is the damping constant. The damping force arises from Stokes drag with the assumption of the existence of fluid in the cell, as in the experiment of Rietz *et al.* We consider two forms for $\vec{v}_{\rm fluid}$ for the Stokes drag in Supplemental Material, Sec. B.3 [20]. The equations of motion are integrated using a modified velocity-Verlet scheme. The simulations are carried out in the hard-sphere limit for the grains, as discussed in Sec. B.2 of Ref. [20].

To shear the packing, the bottom wall oscillates in the $x$ direction [see Fig. 1(a)] as the two sidewalls tilt with an angle $\theta$ that evolves with time $t$ as $\theta(t) = A\sin(\omega t)$, where $A$ is the shear amplitude and $\omega = \pi$ rad/s is the angular frequency. We study shear amplitudes $A = 0.03$, 0.04, 0.05, 0.0667, 0.0833, and 0.10 rad. The oscillating bottom wall is subjected to a force $\vec{F}_{b,j}$ from interior grains. The motion of the bottom wall in the presence of the applied pressure $P$ can be obtained by solving

$$M\vec{a}_b = \sum_{j=1}^{N_b}\vec{F}_{b,j} - b(\vec{v}_b - \vec{v}_{\rm fluid}) - Mg\hat{y} + L^2P\hat{y}, \tag{3}$$

where $M$ is the total mass of the bottom wall, $N_b$ is the number of interior particles that are in contact with the bottom wall, $\vec{v}_{\rm fluid}$ is discussed in Supplemental Material, Sec. B.3 [20], and $\vec{a}_b$ and $\vec{v}_b$ are the acceleration and velocity of the bottom wall, which are constrained to move along the direction $\hat{n} = [\sin\theta(t), \cos\theta(t), 0]$ at time $t$.

*Results.*—The global volume fraction $\phi$ of a collection of grains in a container is the sum of the volumes of the grains divided by the volume of the container. If one partitions the volume of the container into the Voronoi cells of the grains [21], one can define the local volume fraction $\phi_{\rm local}$ for each Voronoi cell or grain. Then for a collection of grains, $\phi$ is the mean of $\phi_{\rm local}$ for all of the grains that are not fixed on the boundary.

The results for $\phi$ for shear amplitudes $A = 0.03$, 0.04, 0.05, 0.068, 0.083, and 0.10 rad are shown in Fig. 1(c), along with results from the experiment [9] for $A = 0.01$ rad. For each shear amplitude, $\phi$ increases in a similar way for the first few shear cycles, while subsequently the increase in $\phi$ is more rapid for larger shear amplitudes, as observed in earlier experiments [7,8].

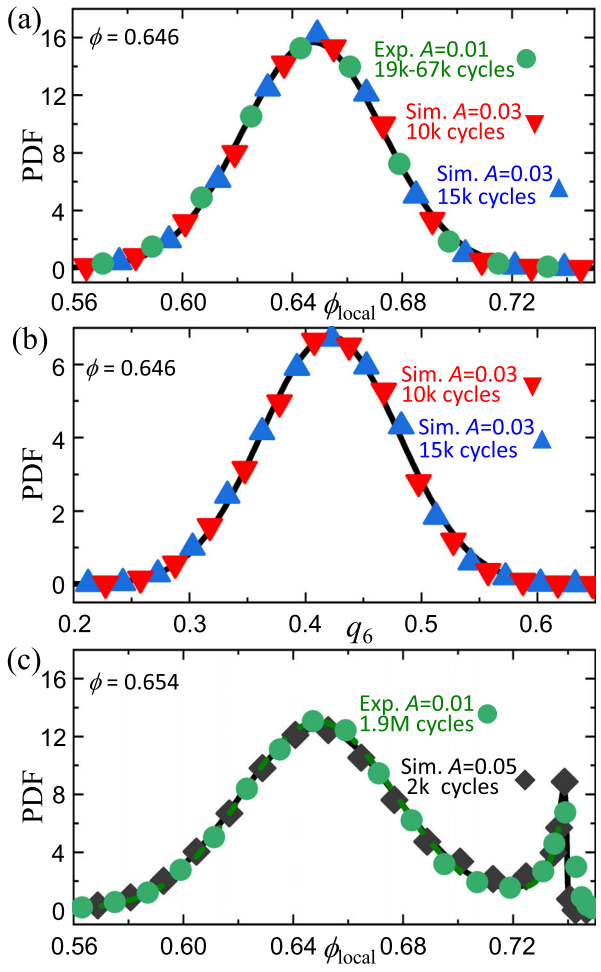


FIG. 2. The probability distribution function (PDF) of (a) the local volume fraction $\phi_{\text{local}}$ and (b) the local bond orientational order parameter $q_6$. Each PDF is time invariant during the range of simulation shear cycles shown, and the experimental data [9] in (a) are also time invariant for a wide range of shear cycles. The black curves in (a) and (b) are Gaussian fits to the PDFs. (c) At this larger global volume fraction, the PDF for $\phi_{\text{local}}$ from both simulations and experiment contains a second peak at $\phi_{\text{local}} = 0.74$, which corresponds to crystallites that have formed with HCP and FCC symmetries, as determined from analyses of particle positions. The black curve is a fit of the data to the sum of a Gaussian $g(x)$ and an inverse Gaussian (i.e., a Wald distribution), $f(x)$: $P(\phi) = ag(\phi_{\text{local}}) + (1-a)f(\phi_c - \phi_{\text{local}})$, where $\phi_c = \pi/3\sqrt{2} \approx 0.7405$.

At low shear amplitudes and for sufficiently small cycle numbers, the system remains disordered. Figure 2(a) shows, for $A = 0.03$ rad at 10 000 cycles and at 15 000 cycles, probability distribution functions (PDFs) for the local volume fraction $\phi_{\text{local}}$. The PDFs become time invariant after ~10000 shear cycles. Figure 2(b) shows time invariance also in the PDFs for the local bond orientational order $q_6$ [22], which we use to identify crystallization (see Supplemental Material, Sec. A [20]). Similarly, the experiment with $A = 0.01$ rad reached a persistent state at $\sim 10^5$ shear cycles [see Fig. 1(c)].

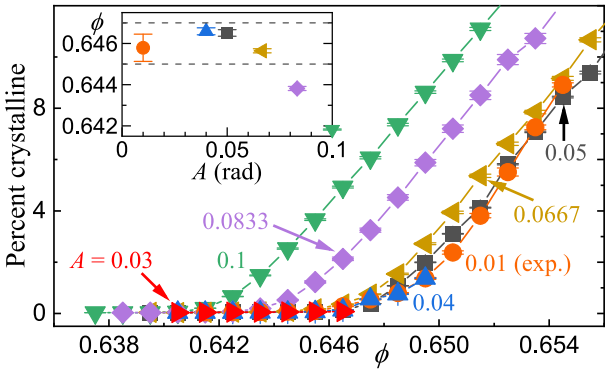


FIG. 3. The percentage of spheres in crystallites as a function of the volume fraction is shown for simulations with $A = 0.03$ to 0.10 rad and an experiment with $A = 0.01$ rad; the horizontal bars on the data points show the standard error of the mean. The results from the simulation with $A = 0.05$ rad and the experiment with $A = 0.01$ rad are remarkably similar. The inset shows that for sufficiently small $A$, $\phi_{\text{onset}} = 0.646 \pm 0.001$.

The simulations with amplitudes $A \geq 0.04$ rad do not give rise to a persistent state [see Fig. 1(c)]. As $\phi$ increases with increasing shear cycling, the height of the peak in the PDF at $\phi_{\text{local}} \approx 0.65$ begins to decrease and another peak emerges at $\phi \approx 0.74$, as shown in Fig. 2(c) for the simulation with $A = 0.05$ rad and the experiment with $A = 0.01$ rad.

Figure 3 presents results for the fraction of the system that is crystalline in simulations with different amplitudes $A$. (The identification of crystalline grains is discussed in Supplemental Material, Sec. A [20].) The similarity between the results from the simulation for $A = 0.05$ rad and the experiment for $A = 0.01$ rad is remarkable considering the many differences between the simulation model and the laboratory experiment. For $A > 0.05$ rad (i.e., 0.067, 0.083, and 0.10 rad), the crystallization onset decreases with increasing $A$ (see Fig. 3).

The inset of Fig. 3 shows that in the limit of small shear amplitude $A$, the crystallization onset is at $\phi = 0.646 \pm 0.001$. In Supplemental Material, Sec. C [20] we show that an alternative method for determining the volume fraction at the onset of crystallization, i.e., when the largest crystallite reaches the critical cluster size (~10 grains), yields a result in agreement with that in Fig. 3. Figure 4 presents results that show that crystallites with more than about 10 grains tend to grow while smaller crystallites tend to shrink.

Most of our simulations were conducted with continuous shear (continuously moving side walls), but some simulations were conducted with periodically paused shear, where grains were allowed to come to rest after each oscillation cycle. Figure 5(a) shows that the results for $\phi$ as a function of shear cycle number are the same initially for the two cases, but differ slightly beyond the onset of crystallization (indicated by the shaded horizontal bar).

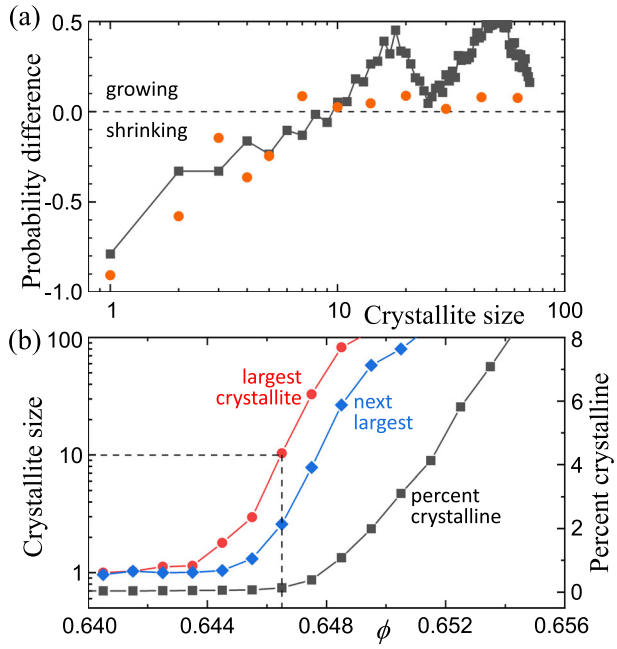


FIG. 4. (a) The difference between the probability that a crystallite will grow rather than shrink during cyclic shear, from simulations with amplitude $A = 0.05$ rad (black squares) and from an experiment with $A = 0.01$ rad (orange circles); in both cases crystallites with more than 10 spheres tend to grow while smaller crystallites tend to disappear. (b) The largest crystallite, the next largest crystallite, and the percentage of spheres in crystallites as a function of the global volume fraction for simulations with shear amplitude $A = 0.05$ rad; the data were averaged over 10 simulations with different initial conditions.

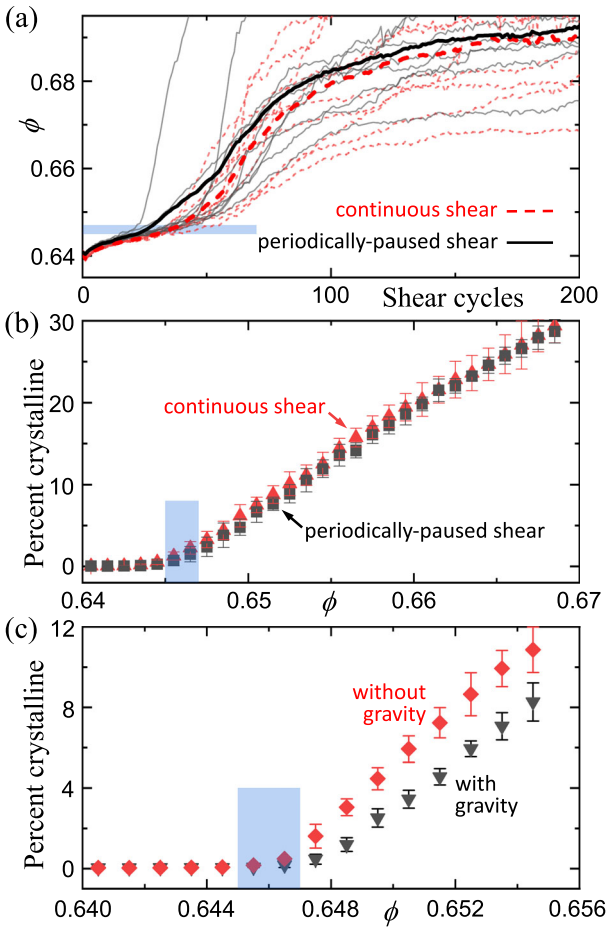


FIG. 5. (a) Global volume fraction as a function of the cycle number during cyclic shear with amplitude $A = 0.0833$ rad for ten simulations with continuous shear (red dashed line) and ten simulations with a periodically paused shear protocol (black solid line) (see Supplemental Material, Sec. B.5 [20]). The light blue bars in (a), (b), and (c) show the standard deviation $\pm 0.001$ in the onset of crystallization at $\phi = 0.646$. (b) The percentage of spheres in crystallites as a function of $\phi$ for the simulations in (a). (c) The percentage of spheres that are in crystallites as a function of $\phi$ for simulations with and without gravity at $A = 0.05$ rad. The vertical bars on the data points in (b) and (c) show the standard deviation. In each panel, the shaded gray rectangle shows the volume fraction for the onset of crystallization, $\phi = 0.646 \pm 0.001$.

However, the focus of our work is on the crystallization fraction as a function of $\phi$, which is the same for continuous and periodically paused shear, as Fig. 5(b) illustrates. Further, Fig. 5(c) shows that gravity plays a negligible role in determining the onset of crystallization.

*Discussion*.—Our simulations of the deterministic equations of motion for frictionless monodisperse spheres in a container undergoing periodic shear reveal that the crystallization onset occurs at a well-defined volume fraction, $\phi = 0.646 \pm 0.001$ (see inset of Fig. 3), in very good agreement with an earlier experiment [9] that was also for small shear amplitude $A$, large system size, and hard-sphere interactions. In our simulations, the dissipation arose only from Stokes drag on the spheres, while in the experiment dissipation arose from static and dynamic friction between grains in contact, inelasticity of the grains, and Stokes drag on the motion of the grains in the viscous fluid surrounding the grains.

The random close packed (rcp) limit has never been unambiguously defined and may well be different for different physical compaction protocols [23–25]. The well-defined value of the global volume fraction that we find at the onset of crystallization is robust to friction, gravity, and amplitude changes in the small amplitude limit. Our value, $\phi = 0.646 \pm 0.001$, is in the reported range for rcp, 0.62–0.66 [26–30]. To avoid confusion we refer to the value we obtain as the "crystallization volume fraction" for asymptotically small shear amplitudes.

For compaction protocols such as cyclic shear coupled with horizontal and vertical shaking, the particles possess significant kinetic energy that is slowly drained during the compaction process. For such protocols, the volume fraction at the onset of crystallization may occur at a different value than the one found here. One method to investigate

this question is to carry out simulations of cyclic shear for underdamped, frictionless grains with weak damping, in addition to weak horizontal vibrations. Then the onset of crystallization could be determined as a function of the damping coefficient [31] as well as in the limit of small shear and vibration amplitudes.

Experiments and simulations of crystallization in non-granular systems, in particular the homogeneous freezing of molecular fluids [17,18], should be compared with the homogeneous crystallization in the present simulations and in Rietz *et al.* [9,32]. For example, persistent states play an important role in classical nucleation theory, but seem to play a marginal role in these simulations and experiment, disappearing with growing shear amplitude.

We acknowledge support from NSF Grants CBET-2002782 (C. O.), CBET-2002797 (M. S.), and DMR-1119826 (W. J.) and Army Research Laboratory Grant W911NF-17-1-0164 (C. O.). This work was also supported by the High Performance Computing facilities operated by Yale's Center for Research Computing and computing resources provided by the Army Research Laboratory Defense University Research Instrumentation Program Grant No. W911NF1810252.

*microwei.jin@gmail.com

[1] J. D. Bernal, A geometrical approach to the structure of liquids, Nature (London) **183**, 141 (1959).
[2] G. D. Scott, Packing of equal spheres, Nature (London) **188**, 908 (1960).
[3] J. B. Knight, C. G. Fandrich, C. N. Lau, H. M. Jaeger, and S. R. Nagel, Density relaxation in a vibrated granular material, Phys. Rev. E **51**, 3957 (1995); P. Richard, M. Nicodemi, R. Delannay, P. Ribiere, and D. Bideau, Slow relaxation and compaction of granular systems, Nat. Mater. **4**, 121 (2005).
[4] S. R. Liber, S. Borohovich, A. V. Butenko, A. B. Schofield, and E. Sloutskin, Dense colloidal fluids form denser amorphous sediments, Proc. Natl. Acad. Sci. U.S.A. **110**, 5769 (2013).
[5] K. Chen, J. Cole, C. Conger, J. Draskovic, M. Lohr, K. Klein, T. Scheidemantel, and P. Schiffer, Packing grains by thermal cycling, Nature (London) **442**, 257 (2006).
[6] M. Schröter, D. I. Goldman, and H. L. Swinney, Stationary state volume fluctuations in a granular medium, Phys. Rev. E **71**, 030301 (2005).
[7] G. D. Scott, A. M. Charlesworth, and M. K. Mak, On the random packing of spheres, J. Chem. Phys. **40**, 611 (1964).
[8] M. Nicolas, P. Duru, and O. Pouliquen, Compaction of a granular material under cyclic shear, Eur. Phys. J. E **3**, 309 (2000).
[9] F. Rietz, C. Radin, H. Swinney, and M. Schröter, Nucleation in Sheared Granular Matter, Phys. Rev. Lett. **120**, 055701 (2018).
[10] M. Saadatfar, H. Takeuchi, V. Robins, N. Francois, and Y. Hiraoka, Pore configuration landscape of granular crystallization, Nat. Commun. **8**, 15082 (2017).
[11] K. E. Avila, H. E. Castillo, A. Fiege, K. Vollmayr-Lee, and A. Zippelius, Strong Dynamical Heterogeneity and Universal Scaling in Driven Granular Fluids, Phys. Rev. Lett. **113**, 025701 (2014).
[12] L. Berthier and J. Kurchan, Non-equilibrium glass transitions in driven and active matter, Nat. Phys. **9**, 310 (2013).
[13] J. Plagge and C. Heussinger, Melting a Granular Glass by Cooling, Phys. Rev. Lett. **110**, 078001 (2013).
[14] G. Castillo, N. Mujica, and R. Soto, Fluctuations and Criticality of a Granular Solid-Liquid-Like Phase Transition, Phys. Rev. Lett. **109**, 095701 (2012).
[15] W. T. Kranz, M. Sperl, and A. Zippelius, Glass Transition for Driven Granular Fluids, Phys. Rev. Lett. **104**, 225701 (2010).
[16] A. Baule, F. Morone, H. Herrmann, and H. Makse, Edwards statistical mechanics for jammed granular matter, Rev. Mod. Phys. **90**, 015006 (2018).
[17] F. F. Abraham, *Homogeneous Nucleation Theory* (Academic Press, New York, 1974).
[18] P. Debenedetti, *Metastable Liquids* (Princeton University Press, Princeton, NJ, 1996).
[19] P. Chaudhuri, L. Berthier, and S. Sastry, Jamming Transitions in Amorphous Packings of Frictionless Spheres Occur Over a Continuous Range of Volume Fractions, Phys. Rev. Lett. **104**, 165701 (2010).
[20] See Supplemental Material at http://link.aps.org/supplemental/10.1103/PhysRevLett.125.258003 for discussions of the identification of the crystalline grains (Sec. A), the computational method (including a list of parameters for the simulation, Sec. B.1), the dependence on the spring constant magnitude (Sec. B.2), drag force (Sec. B.3), simulation timestep size (Sec. B.4), the protocol used for energy relaxation (Sec. B.5), the setup of the shear cell (Sec. B.6), the determination of the critical cluster size (Sec. C), the role of gravity (Sec. D), and the homogeneity of the nucleation process (Sec. E).
[21] A. Okabe, B. Boots, K. Sugihara, and S. N. Chui, *Spatial Tessellations: Concepts and Applications of Voronoi Diagrams*, 2nd ed. (John Wiley & Sons, Chichester, 2000).
[22] P. J. Steinhardt, D. R. Nelson, and M. Ronchetti, Bond-orientation order in liquids and crystals, Phys. Rev. B **28**, 784 (1983).
[23] S. Torquato, T. M. Truskett, and P. G. Debenedetti, Is Random Close Packing of Spheres Well Defined? Phys. Rev. Lett. **84**, 2064 (2000).
[24] C. Radin, Random close packing of granular matter, J. Stat. Phys. **131**, 567 (2008).
[25] Y. Jin and H. A. Makse, A first-order phase transition defines the random close packing of hard spheres, Physica (Amsterdam) **389A**, 5362 (2010).
[26] G. D. Scott and D. M. Kilgour, The density of random close packing of spheres, J. Phys. D **2**, 863 (1969).
[27] J. L. Finney, Random packings and the structure of simple liquids I. The geometry of random close packing, Proc. R. Soc. A **319**, 479 (1970).
[28] J. G. Berryman, Random close packing of hard spheres and disks, Phys. Rev. A **27**, 1053 (1983).

[29] T. Aste, M. Saadatfar, and T. J. Senden, Geometrical structure of disordered sphere packings, Phys. Rev. E **71**, 061302 (2005).

[30] V. Baranau and U. Tallarek, Random-close packing limits for monodisperse and polydisperse hard spheres, Soft Matter **10**, 3826 (2014).

[31] S. S. Ashwin, J. Blawzdziewicz, C. S. O'Hern, and M. D. Shattuck, Calculations of the basin volumes for mechanically stable packings, Phys. Rev. E **85**, 061307 (2012).

[32] C. Radin and H. L. Swinney, Phases of granular matter, J. Stat. Phys. **175**, 542 (2019).